Adaptive Critics with Spiking Neural Networks for Applications in Smart Power Grids

Pinaki Mitra and Ganesh K. Venayagamoorthy

Real-Time Power and Intelligent Systems Laboratory, Missouri University of Science & Technology, Rolla, MO -65409, USA

Abstract:

The smart grid enables us to integrate, interface with and intelligently control the conventional as well as renewable energy resources. The conventional controllers are no longer capable to handle the complexity of smart grids because they are local and non-coordinated controllers. Therefore, wide-area monitoring and control has become important in smart grid related research. In recent years, Adaptive Critic Design (ACD) based optimal wide-area neurocontroller has been proven effective to improve the stability of power systems. But, Multi-Layered Perceptron which is generally used in the framework of adaptive critic does not actually represent the structure and function of biological neural networks. The artificial neural network designed to more closely model the behavior of the biological neural network is known as Spiking Neural Network (SNN). The objective of this research is to design an ACD based wide area controller for a smart grid including a wind farm and six plug-in electric vehicle parking lots. Inside the ACD based controller, the model network is replaced by the SNN. The performance of the controller is evaluated in real-time with Real Time Digital Simulator (RTDS) and DSP based experimental setup.

Introduction:

With the advent of twenty-first century, the limitations of traditional power grids are being revealed day by day. They are lacking in efficiency, reliability, security and above all they are not environment-friendly. Therefore the thrust of the global research has been shifted to a new concept of power grid which is referred as 'the smart grid'. The smart grid encompasses the technology that enables us to integrate, interface with and intelligently control the conventional as well as renewable energy sources like wind farms, solar farms, and the plug-in electric vehicles (PEV) [1]. But, the operational problems originated due to the addition of intermittent sources like wind farms and the congestions created by the charging load of the PEVs are the biggest challenge to the smart grids [2].

The standard power system controllers are no longer capable to handle these problems because; in most cases they are local non-coordinated controllers and try to achieve a local optimal performance but have little or no information about the entire system performance. Even, sometimes, the interactions between these local controllers create adverse effects on the system [3]. These are the reasons why the wide-area monitoring and control (WAMC) is becoming so important in smart grid related research. WAMC has shown significant improvement in damping inter-area oscillations by providing external control signals to the power system stabilizers (PSSs) and different FACTS devices like static VAR compensators (SVC), thyristor-controlled series capacitor (TCSC), unified power flow controller (UPFC) and static compensator (STATCOM) [4]-[7].

The main problem with the classical wide area controllers is that they need a detailed model of the system linearized around a nominal operating point. But with power electronics based devices, it is very difficult to obtain a linearized model of a large system. Also, the operating point for a large power system

is never constant. Due to these reasons, potential of the intelligent nonlinear controllers, which are less sensitive to operating points, are being investigated by many researchers. Among different intelligent techniques, Neural Network has shown its promise in the area of control of power systems as well as the FACTS devices [8]-[9]. But, most of the neural network based controllers are suboptimal controllers and hence provide no guarantee about the system stability unconditionally. In recent years, Adaptive Critic Design (ACD) based optimal wide-area neurocontroller has been proven effective to improve the stability of power systems [10]-[12].

Generally, the basic structure of the neural networks used so far in the framework of adaptive critic is Multi-Layered Perceptron (MLP). But with the advancement of neuroscience it has become clear to the researchers that MLP does not actually represent the structure and function of biological neural networks [13]. A traditional neuron in MLP uses weighted multipliers and simple summation to generate a net input value for an activation function, whose output is the neuron's output. Whereas, a biological neuron receives the fast action potential spikes, which drive up the voltage on its main body's membrane. The voltage on the main body (called the "soma") decays quickly, but if enough spikes arrive (usually from multiple neurons) in a short enough period of time, the biological neuron fires [14]. The artificial neuron designed to more closely model those found in nature is known as a Spiking Neuron, and a network based upon them is called Spiking Neural Network (SNN). Theoretically, due to the close similarity with the biological neural network, the scalability and processing speed of SNN should be much higher than conventional MLPs. Recently the SNN has been proven effective in function approximations and neuroidentification [13]-[15], but its potential in neurocontrol is not yet explored. This research will be the first attempt to investigate the potential of SNN in optimal neurocontrol with ACD.

The objective of this summer research is to design an ACD based wide area controller for a smart grid including a wind farm and six PEV parking lots. The goal of the controller will be: a) to improve the fault tolerance of the system, b) to coordinate the reactive power supplied by the wind farm and the PEVs to improve the voltage stability of the system. Inside the ACD based controller, the model network is replaced by the SNN. The performance of the controller is evaluated in real-time with the test system simulated in Real Time Digital Simulator (RTDS) and the controller being implemented inside a DSP.

Modeling of the Test System:

A. Modeling of the overall system

The overall test system including the wind farm and the plug-in vehicle parking lots is presented in Fig. 1. The 12-bus system was proposed in [16] to evaluate the effects of FACTS devices in the transmission level. The system has four generators and three interconnected areas. Generator G1 represents the infinite bus. In a typical city, there will be several PEV parking lots distributed throughout the city in distances of one to few kilometers. In order to represent this, six three-phase PEV parking lots (PL1 to PL6) are added to this system in Area 2 to bus 13. Bus 13 is an additional bus added to the original 12-bus system in order to connect the PEV parking lots. Bus 13 is connected to bus 6 through 22 kV/230 kV step-up transformers.

B. Modeling of the wind farm

The wind farm is equipped with a Doubly Fed Induction Generator. It uses back-to-back PWM converters for variable speed wind power generation. The control objective of the grid side converter is to keep the dc link voltage constant regardless of the magnitude and direction of the rotor power. A stator oriented vector control approach is used where the direct axis current is used to control the dc link voltage and the quadrature axis current is used to control the reactive power and in turn the voltage at the point of common coupling. The control strategy is similar to [17]. The objective of the rotor side converter is to control the active and reactive power from the stator. This is achieved by putting the d-axis of the rotor

reference frame along the stator flux vector. The q-axis current reference is generated directly from the commanded electrical power and the d-axis current reference is generated from the stator reactive power command. The electrical power command is generated from the optimum operating point tracking strategy discussed in [17], when the wind speed is below a certain value. The pitch control does not work at that time and the wind turbine captures maximum possible energy at that wind speed. But, if the wind speed goes beyond a certain value, the pitch control limits the power generated by the wind turbine. The figures for the rotor side and grid side converter control, the relevant mathematical equations are mostly similar to [17] and hence not included in this report. The data for the 400 MW wind farm is taken from [18].

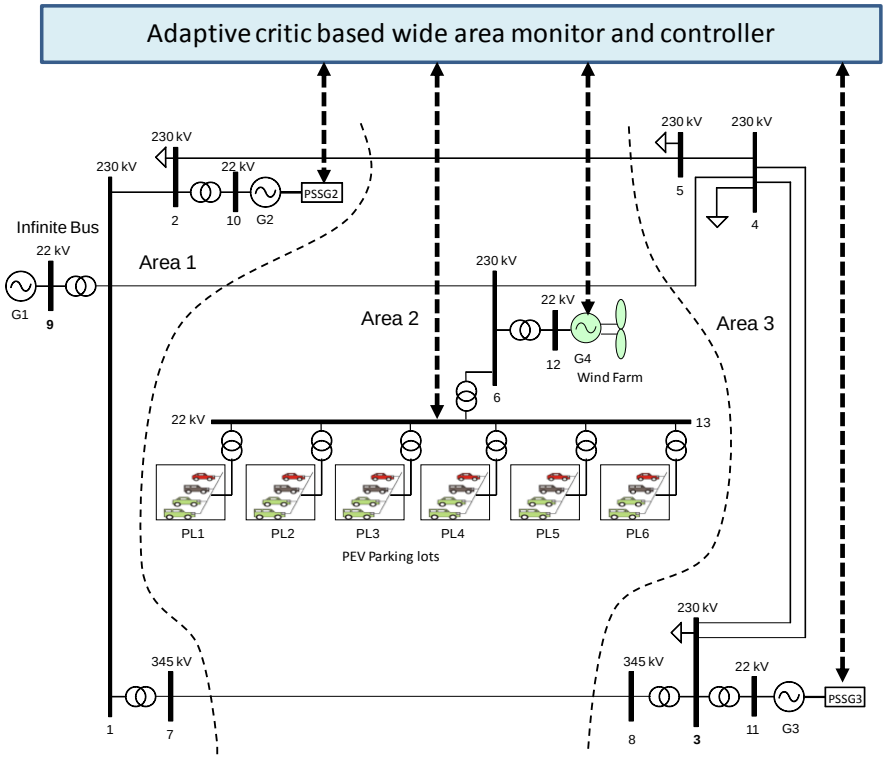

Fig. 1. Overall Test System

C. *Modeling of the plug-in vehicle parking lot*

The parking lot model in this paper is represented by a battery followed by a bidirectional three phase inverter. The inverter generates a 2.08 kV three phase line-to-line rms voltage which is then passed through a 2.08kV/22kV step up transformer and connected to the smart park bus (bus-13 in Fig. 1). Between the inverter and the transformer there is a small (0.5mH) inductance. The control of the inverters is designed in such a way that each inverter can draw ±20 MW of active power. Considering each vehicle can draw ±25 kW, each parking lot in this paper represents 800 vehicles aggregated together. Here '+' sign means the vehicles are selling power to the grid, i.e. they are in discharging mode and the '-' sign indicates that they are buying power from the grid, that means the vehicles are in charging mode. The control strategy for the PEV is presented in Fig. 2. In *d-q* reference frame, the active and reactive powers coming out of the inverter are:

$$P_e = \frac{3}{2}\left(v_{qs}^e i_{qs}^e + v_{ds}^e i_{ds}^e\right) \tag{1}$$

$$Q_e = \frac{3}{2}\left(v_{qs}^e i_{ds}^e - v_{ds}^e i_{qs}^e\right) \tag{2}$$

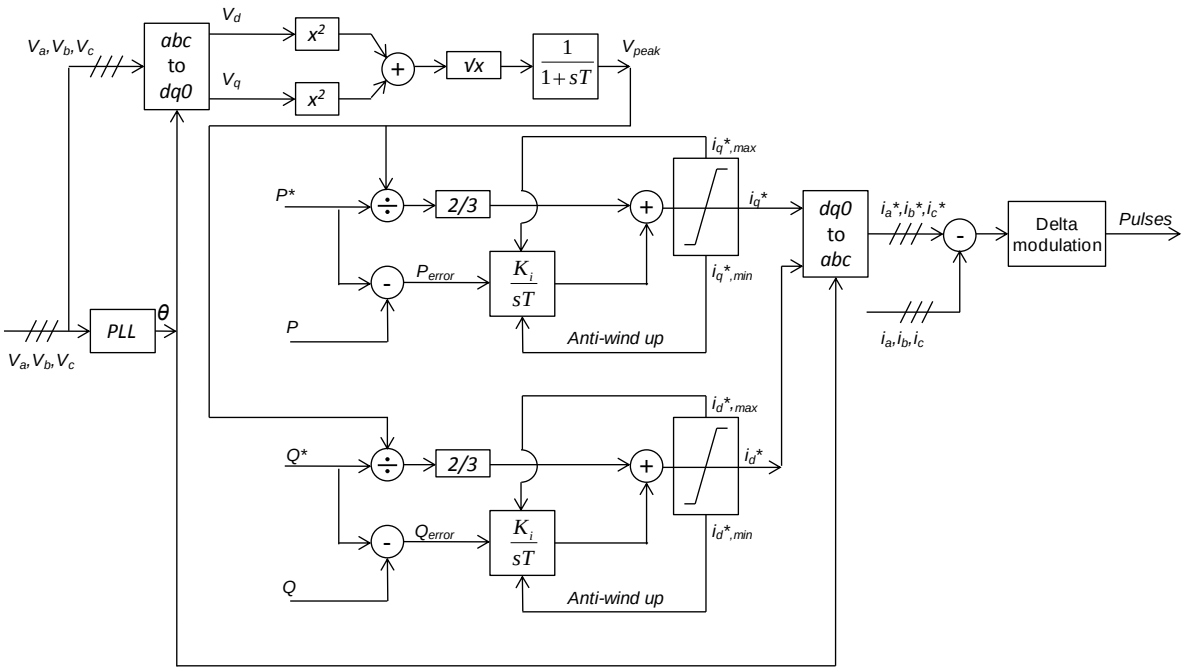

Fig. 2. The current control strategy for the plug-in vehicle parking lots

In synchronous reference frame the peak line-to-neutral voltage is in the *q*-axis and $v_{ds}^{e} = 0$. Therefore, the basis of the control is to command the currents in response to demanded power as

$$i_{qs}^{e*} = \frac{2}{3}\frac{P_e^*}{\sqrt{2}\tilde{V}_s} + \frac{K_i}{s}\left(P_e^* - P_e\right) \tag{3}$$

$$i_{ds}^{e*} = \frac{2}{3}\frac{Q_e^*}{\sqrt{2}\tilde{V}_s} + \frac{K_i}{s}\left(Q_e^* - Q_e\right) \tag{4}$$

The first component of (3-4) is based on the power equations (1-2) where $\tilde{V}_s$ is a filtered version of the line-to-neutral rms voltage. This portion creates quick response to sudden changes in commanded power. The integral term trims out the steady-state error. As shown in Fig. 2, a limit is placed on the commanded current and this is used to prevent integrator windup. The commanded *q*- and *d*-axis currents are then transformed to *a*-*b*-*c* variables where delta current-regulation is used to control the converter transistor switches.

The entire system is modeled on a real-time digital simulator (RTDS) platform. The simulation of the DFIG, the rotor side and grid side inverters and the vehicle inverters – all are carried out on the giga processor RTDS cards using small time step (1.5 μs) simulation.

Spiking Neural Network:

In most of the engineering applications, the Integrate-and-Fire (IF) model of biological neuron has been used as the computational unit. In IF model, the real-valued input can be encoded by the interval between the successive spikes which is also known as Inter Spike Interval (*ISI*). In [19], it has been shown that in a temporally encoded IF model, the computational information is present in both mean and

variance of the synaptic input. This type of computational unit has advantage over the perceptron like classical units because, if there are equal amount of excitatory and inhibitory inputs to the neuron, the mean effect on the model is zero. But, with the spike-rate model mentioned above, if the mean vanishes, still the information remains in the variance and there is no problem with the firing of the unit. In this work, the spiking neuron model introduced in [13], is used in a feedforward network and is explained here. The inputs from the previous layer are collected and aggregated by (5) and (6) to generate the mean and standard deviation of the membrane potential over the time-slice represented by a given epoch.

$$\mu_i = \sum_{j=1}^{n} \lambda_j - \lambda^i \quad w_{ij} \quad 1-r \tag{5}$$

$$\sigma_i^2 = \left(\sum_{j=1}^{n} \lambda_j^{\alpha} - \lambda^i \quad w_{ij}^2 \right) 1-r \quad + \rho \sum_{j \neq k=1}^{n} \left(\lambda_j^{\frac{\alpha}{2}} - \lambda^i \right) \left(\lambda_k^{\frac{\alpha}{2}} - \lambda^i \right) w_{ij} w_{ik} \quad 1-r \tag{6}$$

The j^{th} input into the system is λ_j, α is a tuning constant greater than zero, and r is the ratio of excitatory to inhibitory inputs. The superscripted λ values are centers, used to offset a given neuron in much the way a radial basis function (RBF) works. The weights connecting neuron j to input i are given by the subscripted w values. This unique structure allows for an equal number of excitatory and inhibitory inputs (caused when $r = 1$) to not completely damp out the neuron's ability to generate meaningful output [13]. The actual output of the neuron is the "firing rate," which serves as the real value the neuron is to be calculating, with no further decoding necessary. To determine this firing rate, two more pieces of information are required: the *ISI*, or inter-spike interval, and the "refractory period" T_{ref}. After a biological neuron fires off a spike due to having its membrane's threshold potential exceeded, the membrane is actually at a lower potential than its resting potential. The refractory period is the amount of time it takes for this potential to rise back to the resting state. The *ISI* is the given by (7), with *g(x)* being Dawson's Integral (given in (8)). The relaxation rate of the neuron – how long it takes for a spike's influence on the membrane potential to fade – is given as τ. V_{rest} and V_{thresh} are the resting and threshold potentials of the membrane, respectively. Finally, (9) shows the calculation of the firing rate output of the neuron, using the carefully-determined *ISI*.

$$ISI = \frac{2}{\tau} \int_{\frac{V_{rest}\tau - \mu_i}{\sigma_i}}^{\frac{V_{thresh}\tau - \mu_i}{\sigma_i}} g(x)dx \tag{7}$$

$$g(x) = e^{x^2} \int_0^x e^{-u^2} du \tag{8}$$

$$f_i(\lambda) = \frac{1}{T_{ref} + ISI} \tag{9}$$

Adaptive Critics Based Wide-Area Controller:

The single-line diagram of the test system is already shown in Fig. 1. Both the PSSs, the wind farm and the PEV parking lot controllers at the local level are designed using standard linear control techniques but are coordinated using the WAMC to improve the as a whole system performance. The WAMC receives remote signals from different devices including the speed deviations of G2 and G3 ($\Delta\omega_2$ and $\Delta\omega_3$ respectively) and the voltage deviation at bus 6 (ΔV_6). These remote signals contain important transient/dynamic information regarding the stability of the system. Based on those signals, the ACD based WAMC produces the control signals for the generators (ΔV_{T2} and ΔV_{T3}), the grid side reactive

power command for the wind farm (ΔQ_g), and the reactive power command for the PEVs ($\Delta Q_{PEV\text{-}1}$ to $\Delta Q_{PEV\text{-}6}$).

The functioning of ACD based neurocontroller is presented in Fig. 3. It has three neural networks: a) the action network or neurocontroller, b) the model network or the neuroidentifier and c) the critic network. The neuroidentifier is based on SNN. The neurocontroller generates the control signals from the delayed values of remote signals. The weights of the neurocontroller are adjusted by backpropagating 1 though the trained critic network to generate $\partial J / \partial Y$ and then passing the derivative through the trained neuroidentifier to obtain $\partial J / \partial A$. The neuroidentifier basically identifies the model of the system from the delayed values of the remote signals and the action generated by the neurocontroller. The identifier predicts the output of the plant one time step ahead so that it can be used by the critic network. The function of the critic network is to approximate the cost-to-go function J of Bellman's equation of dynamic programming given by equation (6), where γ is a discount factor between 0 and 1 and $U(t)$ is utility function. In the training of the critic network, the objective is presented by (7), where $E(t)$ is given by (8).

$$J(t) = \sum_{k=0}^{\infty} \gamma^k U(t+k) \tag{6}$$

$$Min\left(\sum_{t=0}^{\infty} E^2(t) \right) \tag{7}$$

$$E(t) = \gamma \hat{J}(t+1) + U(t) - \hat{J}(t) \tag{8}$$

Here $\hat{J}(t)$ is the estimated cost-to-go by the critic network at time t.

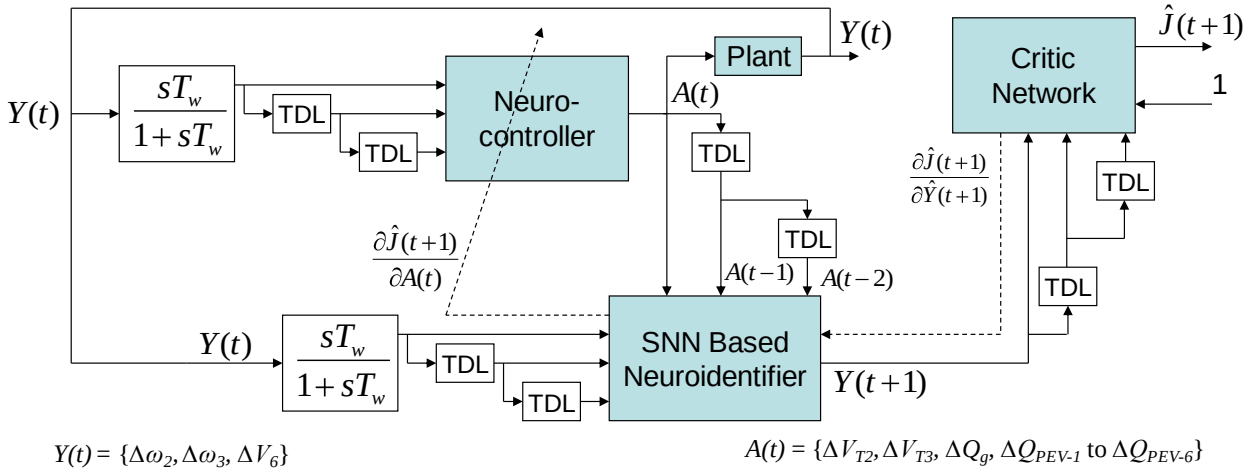

Fig. 3. The Adaptive Critic Design based wide-area controller

Results:

In the first stage, the neuroidentifier is designed using SNN. The time delayed values of the variables Y (*Y(t-1), Y(t-2)* and *Y(t-3)*) and the current and time delayed values of the variables A (*A(t), A(t-1)* and *A(t-2)*) are used to predict the current value of Y (*Y(t)*). In order to excite almost all modes of oscillation, Pseudo Random Binary Signal (PRBS) is applied at the action points. For the sake of simplicity, the reactive power commands of the parking lots are lumped together. This means, six variables $\Delta Q_{PEV\text{-}1}$ to $\Delta Q_{PEV\text{-}6}$ are represented by one variable (ΔQ_{PEV}). Therefore, PRBS is applied at ΔV_{T2}, ΔV_{T3}, ΔQ_g and ΔQ_{PEV}. Since, three time delayed values of each input is used, the total number of input for the SNN is 21. Number of neurons is considered to be 50. The system is run for 30 seconds and 1000 data points are

collected. The parameters of the SNN are considered to be the same as [14]. All the input signals are scaled uniformly within the range of -1 to +1. Fig. 4 shows the identification characteristics by the SNN of the variables $\Delta\omega_2$, $\Delta\omega_3$ and ΔV_6. It is observed that within only 1000 data points, the neuroidentifier can successfully identify the Y variables. The characteristics of one of the PRBS input signal (ΔV_{T2}) is also shown in that figure as an example. Fig. 5 is the zoomed version of Fig. 4. It shows more closely how good the SNN works as an identifier.

In the second stage, adaptive critic based WAC is designed. In order to do that, first the critic is pre-trained keeping the controller parameters constant. Now, the critic parameters are kept constant and the controller is trained. This process is repeated several times upto the point when there is no change in the weights of the controller and the critic network. Once both of them are trained, all the three neural networks are connected to the system with their weights constant.

In order to evaluate the performance of the WAC, the active power commands of the parking lots are suddenly changed in such a way that all of them together discharge a total power of 90 MW to the grid. As a result of this, without any coordinating WAC, the voltage at bus-6 rises to almost 1.03 p.u. from 1.0 p.u. and stays there. But, with WAC, reactive power is injected into the grid from both wind farm and also from PEV parking lots and keep the voltage constant at 1.0 p.u. This is demonstrated in Fig. 6.

In order to show, how the WAC improves the stability of the system, a three phase line to ground fault of 100 ms duration is applied at bus-6. It is observed in Figs. 7-8 that, without WAC, the speeds of the generators start oscillating with the application of the fault. But, with WAC, the speed oscillation of the generators gradually damp out and the system restores to a stable operating condition.

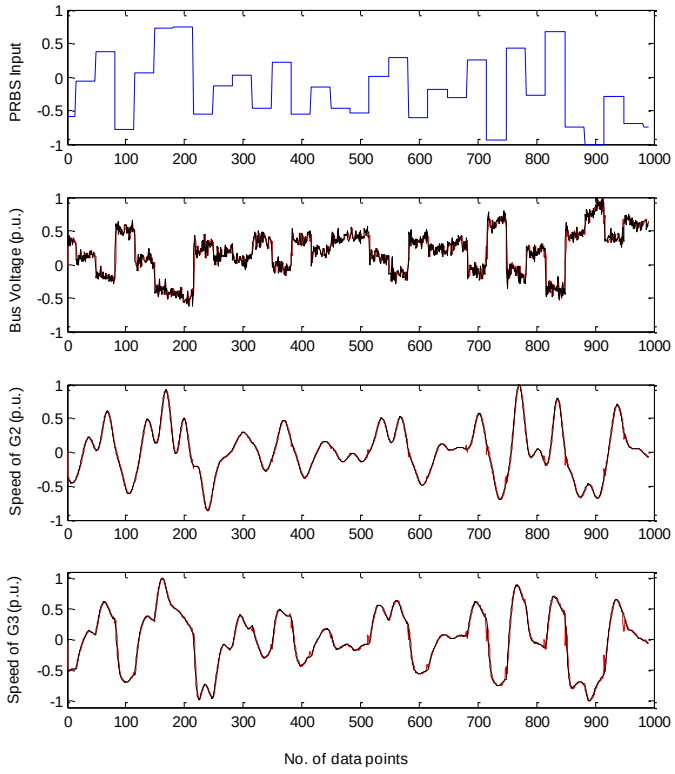

Fig. 4. Identification by SNN

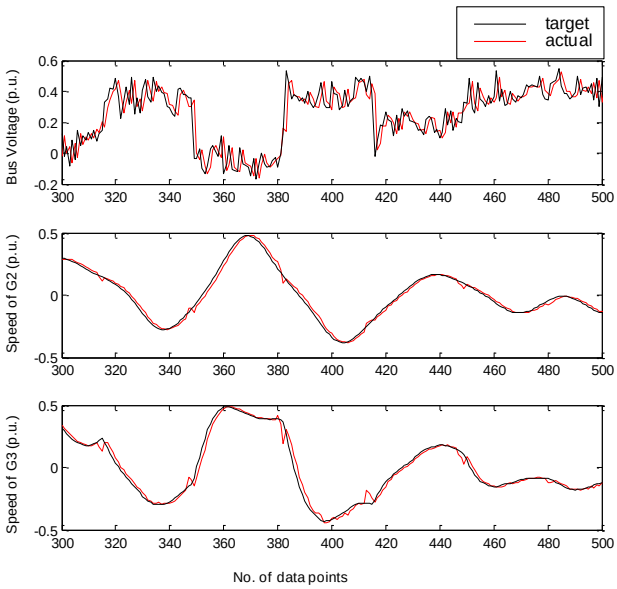

Fig. 5. Zoomed version of Fig. 4

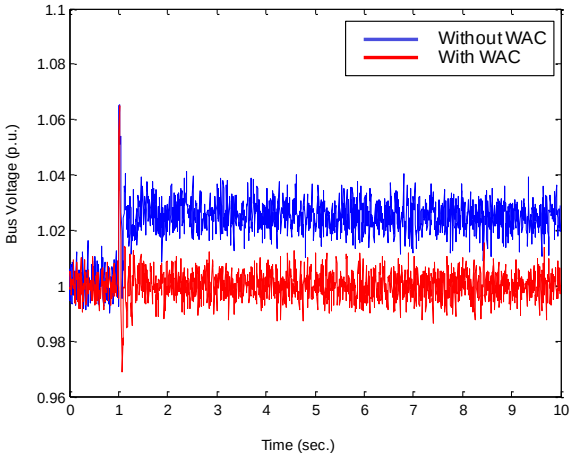

Fig. 6. Voltage characteristics of bus-6

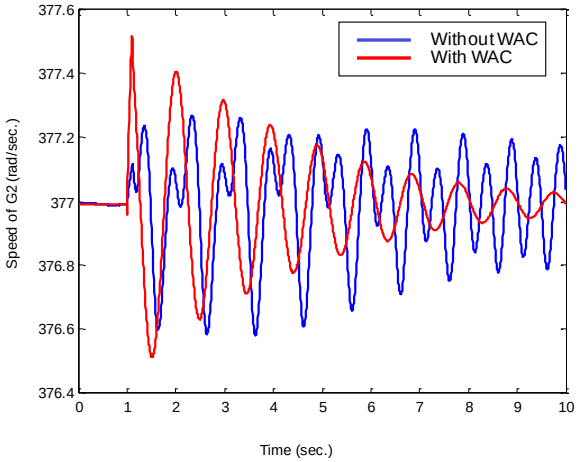

Fig. 7. Speed oscillation of Generator 2

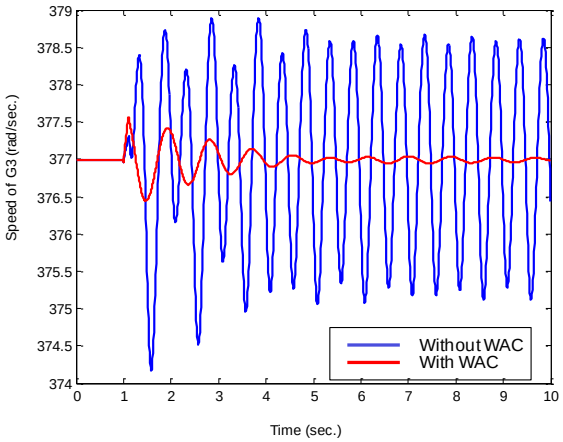

Fig. 8. Speed oscillation of Generator 2

Conclusion:

In this research, a wide-area controller based on adaptive critic design is developed for a smart power grid which includes a large wind farm and six plug-n vehicle parking lots. The adaptive critic based neurocontroller uses the potential of spiking neural network for neuroidentification purposes. The results show that the performance of SNN is very fast and effective in identifying system dynamics from the time delayed values of the inputs and outputs. It is also observed that the wide-area coordinating controller can keep the bus voltage at desired level by varying the reactive power command of the wind farm and the plug-n vehicles. Not only that, it also helps in stabilizing the system in case of a transient disturbance.

In future, the SNN will be used in both the neurocontroller and in the critic network of the adaptive critic framework and its performance will be investigated.

Acknowledgement:

The authors gratefully acknowledge the Walter Karplus Summer Research Grant by IEEE Computational Intelligence Society for funding this project and also the Real-Time Power and Intelligent Systems Laboratory and Missouri University of Science and Technology for providing the infrastructural support for this project.

References:

[1] "The Smart Grid: An Introduction", Prepared for the US Department of Energy by Litos Strategic Communication.

[2] A. Ipakchi and F. Albuyeh, "Grid of the Future", *IEEE Power and Energy Magazine*, vol. 7, issue 2, March – April 2009, pp. 52-62.

[3] W. Qiao, G. K. Venayagamoorthy, R. G. Harley, "Optimal Wide-Area Monitoring and Nonlinear Adaptive Coordinating Neurocontrol of a Power System with Wind Power Integration and Multiple FACTS Devices", *Elsevier Journal of Neural Networks*, issue 21, 2008, pp. 466 – 475.

[4] M. Zima and G. Anderson, "Wide Area Monitoring and Control as a Tool for Mitigation of Cascading Failures", *Proceedings of International Conference on Probabilistic Methods Applications in Power Systems*, Ames, IA, Sep. 12-16, 2004, pp. 663-669.

[5] F. Okou, L. A. Dessaint and O. Akhrif, "Power Systems Stability Enhancement Using a Wide-Area Signals Based Hierarchical Controller", *IEEE Transaction on Power Systems*, vol. 20, no. 3, pp. 1465-1477, Aug. 2005.

[6] S. Ray and G. K. Venayagamoorthy, "Wide-Area Signal Based Optimal Neurocontroller for a UPFC", *IEEE Transaction on Power Delivery*, vol. 23, no. 3, July 2008.

[7] S. Mohagheghi, G. K. Venayagamoorthy, R. G. Harley, "Optimal Wide Area Controller and State Predictor for a Power System", *IEEE Transaction on Power Systems*, vol. 22, no. 2, May 2007, pp. 693-705.

[8] G. K. Venayagamoorthy and S. R. Jetti, "Dual-Function Neuron-Based External Controller for a Static Var Compensator", *IEEE Transaction on Power Delivery*, vol. 23, no. 2, April 2008, pp. 997-1006.

[9] W. Qiao, R. G. Harley, G. K. Venayagamoorthy, "Fault-Tolerant Indirect Adaptive Neuro-Control for a Static Synchronous Series Compensator in a Power Network with Missing Sensor Measurements", *IEEE Transactions on Neural Networks*, Vol. 19, No. 7, July 2008, pp. 1179 - 1195.

[10] S. Ray, G. K. Venayagamoorthy, B. Chaudhuri, R. Majumder, "Comparison of Adaptive Critics and Classical Approaches Based Wide Area Controllers for a Power System", *IEEE Transactions on System, Man and Cybernetics, Part B: Cybernetics*, Vol. 38, No. 4, August 2008, pp. 1002-1007.

[11] W. Qiao, G. K. Venayagamoorthy and, R. G. Harley, "DHP-Based Wide-Area Coordinating Control of a Power System with a Large Wind Farm and Multiple FACTS Devices", *2007 International Joint Conference on Neural Networks*, Orlando, Florida, USA, August 2007, pp. 2093-2098.

[12] S. Ray and G. K. Venayagamoorthy, "Real-time implementation of a measurement-based adaptive wide-area control system considering communication delays", *IET Generation, Transmission and Distribution*, vol. 2, issue 1, January 2008, pp. 62–70.

[13] P. Rowcliffe and J. Feng, "Training spiking neuronal networks with applications in engineering tasks", *IEEE Transactions on Neural Networks*, vol. 19, no. 9, Sept. 2008, pp. 1626-1640.

[14] Johnson, G. K. Venayagamoorthy and P. Mitra, "Comparison of a Spiking Neural Network and an MLP for Robust Identification of Generator Dynamics in a Multimachine System", *Neural Networks, Elsevier Publication*, vol. 22, issue 5-6, July-August 2009, pp. 833-841.

[15] D. Mishra, A. Yadav, S. Ray and P. K. Kalra, "Artificial Neural Network Type Learning with Single Multiplicative Spiking Neuron", *International Journal of Computers, Systems and Signals*, vol. 8, no. 1, 2007, pp. 29-41.

[16] S. Jiang, U. D. Annakkage, and A. M. Gole, "A platform for validation of FACTS models," *IEEE Trans. Power Delivery*, vol. 21, pp. 484–491, Jan. 2006.

[17] R. Pena, J. C. Clare and G. M. Asher, "Doubly Fed Induction Generator Using Back-to-back PWM Converters and its Application to Variable-speed Wind-energy Generation", *IET Proc. Electr. Power Appl*., Vol. 143, no. 3, May 1996.

[18] W. Qiao, R. G. Harley and G. K. Venayagamoorthy, "Coordinated Reactive Power Control of a Large Wind Farm and a STATCOM Using Heuristic Dynamic Programming", *IEEE Trans. Energy Conversion.*

[19] P. Rowcliffe, J. Feng and H. Buxton, "Spiking Perceptions", *IEEE Transaction on Neural Networks*, vol. 17, no. 3, May 2006, pp. 803-807.